Earth and Planetary Science Letters 407 (2014) 70–81

Contents lists available at ScienceDirect

Earth and Planetary Science Letters

www.elsevier.com/locate/epsl

Timing, duration and inversion of prograde Barrovian metamorphism constrained by high resolution Lu–Hf garnet dating: A case study from the Sikkim Himalaya, NE India

Robert Anczkiewicz [a,*], Sumit Chakraborty [b], Somnath Dasgupta [c], Dilip Mukhopadhyay [d], Katarzyna Kołtonik [a]

[a] Institute of Geological Sciences, Polish Academy of Sciences, Kraków Research Centre, Senacka 1, PL 31-002, Kraków, Poland
[b] Institut für Geologie, Mineralogie und Geophysik, Ruhr Universität Bochum, D-44780, Bochum, Germany
[c] Assam University, Silchar - 788 011, Assam, India
[d] Indian Institute of Technology Roorkee, 247667 Roorkee, India

ARTICLE INFO

Article history:
Received 15 May 2014
Received in revised form 17 September 2014
Accepted 20 September 2014
Available online 9 October 2014
Editor: T.M. Harrison

Keywords:
Barrovian metamorphism
garnet geochronology
rates of metamorphism
Lu–Hf
Himalaya
inverted metamorphism

ABSTRACT

We investigated Lu–Hf isotopic systematics in garnets from gradually higher grade metamorphic rocks from the first appearance of garnet at c. 500 °C to biotite dehydration melting at c. 800 °C in the Sikkim Himalaya, India. Exceptionally precise Lu–Hf ages obtained for the Barrovian metasedimentary sequence in the Lesser Himalaya (LH) correspond to the time of early garnet formation on a prograde path and show remarkable correlation with increasing metamorphic grade and decreasing structural depth. The youngest age is reported for the garnet zone (10.6 ± 0.2 Ma) and then the ages become progressively older in the staurolite (12.8 ± 0.3 Ma), kyanite (13.7 ± 0.2 Ma) and sillimanite (14.6 ± 0.1 Ma) zones. The oldest age of 16.8 ± 0.1 Ma was recorded at the top of the sequence in the zone marking the onset of muscovite dehydration melting, directly below the Main Central Thrust (MCT). These ages provide a tight constraint on the timing and duration of the Barrovian sequence formation which lasted about 6 Ma. The age pattern is clearly inverted with respect to structural depth but shows "normal" correlation with the metamorphic grade, i.e. earlier garnet growth in higher grade rocks.

The timing of the peak metamorphic conditions estimated for the garnet and kyanite zones suggests that thermal climax occurred in all zones within a relatively short time span about 10–13 Ma ago. The metamorphic inversion in the Sikkim Himalaya must therefore have occurred after the metamorphic peak was attained in all grades.

Lu–Hf garnet ages in the overthrust Higher Himalaya (HH) continue to be older but do not show a clear progression. There is about 6 Ma jump to 22.6 ± 0.1 Ma within the MCT zone and even older ages of 26–28 Ma were obtained for migmatites from the lower part of the HH. The Lu–Hf system in garnets from the HH records the time of melting at or near the thermal peak rather than dates initial garnet growth as in the LH.

The age pattern obtained in this study provides precise time constraints on the continental collision models which must take into account early and prolonged anatexis in the HH, progressive delay in initial garnet growth in different Barrow zones in the LH, nearly contemporaneous metamorphic peak in all grades and post peak inversion of the coherent LH block during exhumation.

1. Introduction

Understanding the timescales of metamorphic processes is central to our understanding of the thermal evolution of the crust during orogenesis. Metamorphic rocks are thermal probes of the interior of the Earth that have been returned to the surface, and are thus suitable for establishing the timing, duration and rates at which crustal conditions evolve in response to large scale tectonic processes. An exceptionally complete, little disturbed and well preserved Barrovian metasedimentary sequence (Barrow, 1893) in the Sikkim Himalaya provides a unique opportunity to study these fundamental aspects. The tectonic setting is well recognized (the collision of India and Asia) and the basic details of the process such as the age of initiation of collision, rates of convergence, and the gross structural evolution are relatively well known. Most notably,

* Corresponding author. Tel.: +48 12 3705224; fax: +48 12 4221609.
E-mail address: ndanczki@cyf-kr.edu.pl (R. Anczkiewicz).

http://dx.doi.org/10.1016/j.epsl.2014.09.035
0012-821X/

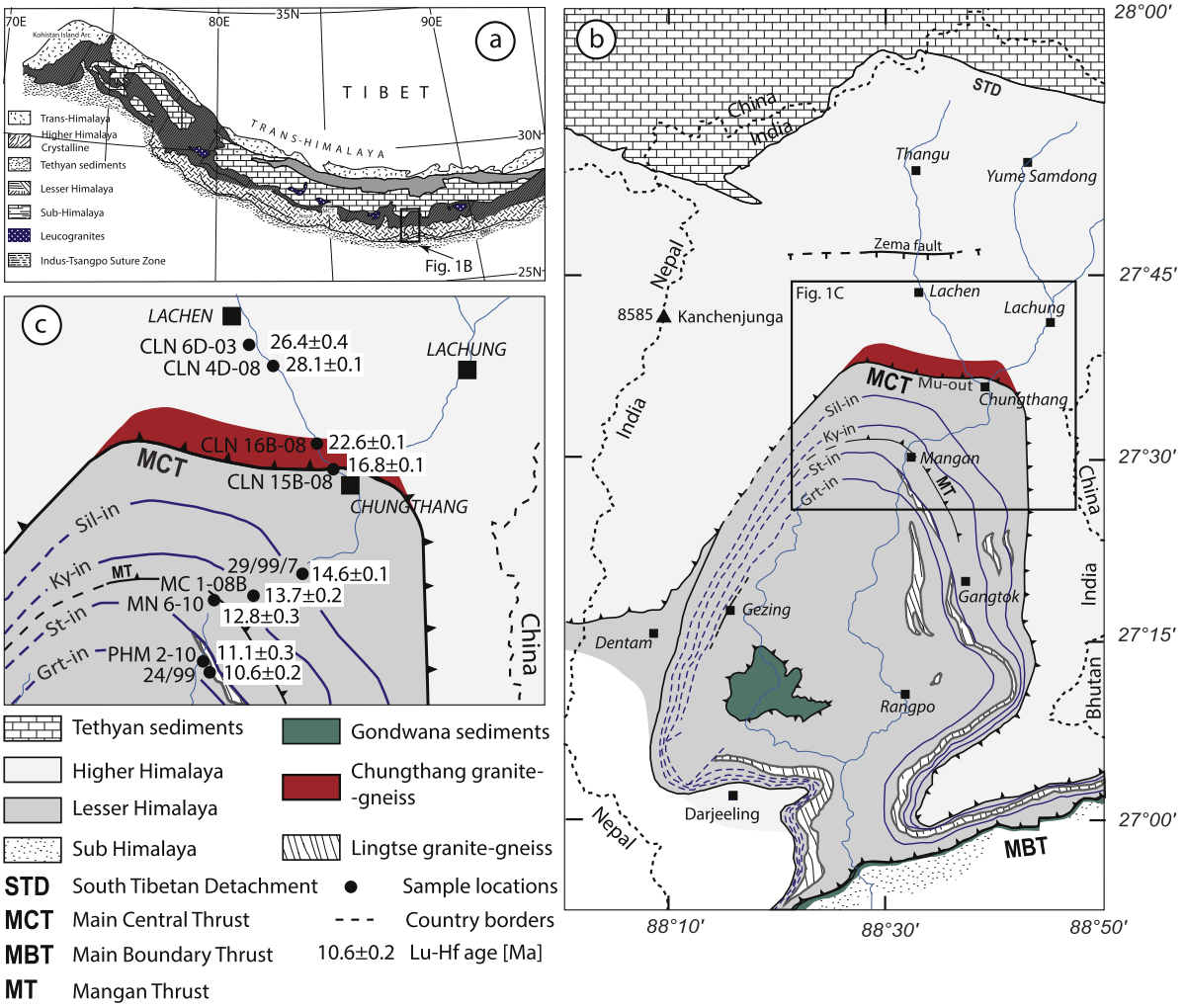

Fig. 1. (a) Geological sketch of the Himalaya (based on compilation from Yin, 2006). The rectangle marks the study area that is enlarged in (b). (b) shows a geological map of Sikkim modified after Mukhopadhyay et al. (in preparation), Ghosh (1956), Acharryya and Ray (1977), Lal et al. (1981) and Ray (2000). The rectangle marks the region that is expanded in (c). Sample locations along with Lu–Hf garnet ages are shown in (c).

the tectono-metamorphic evolution here has been relatively simple in contrast to the situation in other well studied areas such as the Alps or the Barrow's zones in Scotland and in New England, where multiple tectonic events may have affected the rocks or the plate tectonic boundary conditions are less well constrained.

We present precise Lu–Hf garnet growth ages for each Barrovian zone from a well characterized metasedimentary sequence of the Sikkim Himalaya. We provide spatially resolved ages for some garnets so that the dates and their relationship to element zoning as well as to specific stages of garnet growth and metamorphic evolution can be clarified. Additionally, we studied the response of the Lu–Hf isotopic systematics to progressively rising temperature from the first appearance of garnet at c. 500 °C to extensive biotite dehydration melting at c. 800 °C. Finally, we consider the implications of these results for the evolution of the Himalaya and the genesis of inverted metamorphism that is observed all along the Himalaya and in other mountain belts as well.

2. Regional geology

Crustal shortening across the Himalayan range initiated by the India–Asia collision at about 55–50 Ma was accommodated by the major north dipping thrusts, which delineate the main Himalayan structure (Fig. 1a). In the Sikkim state of NE India, the large scale structure closely resembles that of other Himalayan regions. The northernmost part of the Himalaya is composed largely of unmetamorphosed Tethyan sediments bounded by the Indus Suture to the north and the South Tibetan Detachment (STD) to the south. The STD is a north dipping normal fault whose major activity spanned between 17 and 14 Ma (Catlos et al., 2004) or 24 and 13 Ma according to the recent proposal of Kellet et al. (2013). The footwall of the STD exposes strongly metamorphosed and highly deformed Higher Himalayan (HH) rocks, represented primarily by migmatites intruded by leucogranites with subordinate metabasites and calc-silicates. Peak pressure and temperature (PT) conditions of metamorphism appear rather uniform across the entire unit and were determined as 8–10 kbars at about 800 °C (Dasgupta et al., 2009, 2004; Ganguly et al., 2000; Harris et al., 2004; Sorcar et al., 2014). Monazite and zircon U–Pb dating revealed prolonged and diachronous melting across the HH that spanned from 31 to 17 Ma and took place in a series of short (few Ma) episodes (Rubatto et al., 2013). On the basis of different timing of peak temperature conditions and different cooling histories, Rubatto et al. (2013) and Sorcar et al. (2014) distinguished two zones within the HH: 1) north of Lachen, where near peak biotite dehydration melting occurred at 26–23 Ma and cooling was more rapid, and 2) south of Lachen, where major melting happened between 31 and 27 Ma and cooling was slower (Fig. 1b). Additionally, Rubatto et al. (2013) and Sorcar et al. (2014) document a period of melting during prograde heating that led them to conclude that melting

Table 1
Sample locations, mineral assemblages and PT conditions of the studied samples.

Unit	Sample	GPS coordinates	Metamorphic grade	Mineral assemblage	PT conditions
Lesser Himalaya	24/99	N 27°27.292′ E 88°31.63′	Garnet zone	Ms–Chl–Bt–Grt–Qtz–Pl–Ilm	5 kbar, 525 °C[1)]
	PHM2-10	N 27°27.813′ E 88°31.408′	Garnet zone	Ms–Chl–Bt–Grt–Qtz–Pl–Ilm	
	MN6-10	N 27°30.668′ E 88°31.802′	Staurolite zone	Ms–Qtz–Pl–Bt–Grt–St–Ilm–Chl	~5.8 kbar, 540 °C[1)]
	MC1-08	N 27°30.580′ E 88°33.969′	Kyanite zone	Ms-Bt–Qtz–Pl–Grt–Ky–Chl	~6 kbar, 550 °C[1)]
	29/99/7	N 27°31.757′ E 88°36.369′	Sillimanite zone	Qtz–Bt–Ms–Pl–Grt–Sil	6 kbars, 610 °C[1)]
	CLN15B-08	N 27°36.621′ E 88°38.281′	Mu-out zone	Qtz–Pl–Ms–Bt–Grt–Kfs–Sil–Chl (+ retrograde Chl)	6 kbar, 630 °C[1)]
Higher Himalaya	CLN16B-08	N 27°37.913′ E 88°37.201′	Grt granite gneiss	Qtz–Pl–Ms–Bt–Grt–Kfs (+ retrograde Chl)	
	CLN 4D-03	N 27°41.366′ E 88°35.148′	Migmatite	Qtz–Kfs–Pl–Grt–Bt–Sil Retrograde Chl and simplectites	~8 kbar, 780 °C[2)]
	CLN 6D-03	N 27°42.247′ E 88°33.727′	Migmatite	of Spl + Qtz	

Notes: Abbreviations after Kretz (1983). PT conditions marked with a ~ are approximate established by correlating with the same grade rocks from nearby locations. PT data source: [1)] Dasgupta et al. (2009); [2)] Sorcar et al. (2014). Samples 24/99 and 29/99/7 are the same as those used in the study of Dasgupta et al. (2009).

triggered isothermal decompression. This opposes the earlier view of Harris et al. (2004) who proposed that melting within the HH was activated by rapid exhumation between 23 ± 3 and 16 ± 2 Ma.

The southern boundary of the HH is the Main Central Thrust (MCT), one of the most debated structures in the Himalayan geology. The MCT in the Sikkim region has been defined differently by various working groups (Acharryya and Ray, 1977; Catlos et al., 2004; Dasgupta et al., 2004; Ghosh, 1956; Harris et al., 2004; Lal et al., 1981; Ray, 2000; Searle and Szulc, 2005). More recent studies (Mottram et al., 2014; Rubatto et al., 2013; Sorcar et al., 2014) have placed the boundary to the north of the town of Chungthang in the section along the Teesta river and we adopt the same definition here (Fig. 1b, c). On the basis of Th–Pb monazite ages, Catlos et al. (2004) proposed that shearing along the MCT took place in several steps between c. 22 and 10 Ma. The Lesser Himalaya (LH) in the studied section consists of a metasedimentary sequence with local inclusions of metabasites and calc-silicates, as in the HH. The LH expose a complete and rather coherent, inverted Barrovian sequence from chlorite to sillimanite–K-feldspar grade. The metamorphic grade decreases southwards towards structurally deeper levels down to the Main Boundary Thrust (MBT) which places the LH over the mollase deposits (Fig. 1b). The MCT, along with all isograds in its footwall, is folded by the Teesta dome which is the most prominent structure in the Sikkim region (Fig. 1b).

We have focused our study on the LH rocks but have also obtained limited information from the lower part of the HH.

3. Samples and methods

We sampled all garnet bearing zones from the first appearance of garnet in the structurally lowest part, up to the highest metamorphic grade in the structurally highest part of the sequence (Fig. 1c). GPS positions of the sampling locations, mineral assemblages and pressure–temperature conditions of metamorphism are summarized in Table 1. Photomicrographs of samples dated by Lu–Hf method are shown in Fig. 2.

Nearly all samples subjected to isotopic analyses were prepared by routinely used techniques of crushing, sieving, magnetic and heavy liquids separation. Bulk garnet separates were prepared by handpicking the cleanest pieces whose weights ranged from 40 to 100 mg per analyses (Table 2). Only samples PHM2-10 and MC1-08, from which single garnet crystals were dated, underwent different treatment which is outlined below. A single garnet crystal of about 0.5 cm diameter was separated from the matrix minerals of sample PHM2-10, crushed in an agate mortar and split into three random fractions that did not undergo any additional purification prior to chemical digestion. Sample MC1-08 contained exceptionally large, euhedral garnet crystals that were perfectly suited for high spatial resolution dating. We cut a 1.7 mm thick slice through the geometric center of a 3 cm large garnet. The slice was polished and analyzed using the electron microprobe (major elements) and laser ablation ICP-MS (trace elements) before isotopic analyses were carried out. On the basis of the garnet's internal texture and chemical composition we selected three different growth zones for analyses. The selection of these domains is explained below in the section presenting the results of isotopic analyses.

The trace element zoning profiles in garnets from all samples were measured at the Institute of Geological Sciences, Polish Academy of Sciences, Kraków Research Centre using an ArF excimer laser-ablation system *RESOlution M50* by Resonetics (Müller et al., 2009) coupled with quadrupole ICP-MS *XSeriesII* by Thermoelectron. Analytical details follow Anczkiewicz et al. (2012). Sample runs were bracketed by measurements of NIST 612 glass using reference values of Jochum et al. (2011). Silica content was used as an internal standard. Data were processed using Glitter 4.0 software from Macquarie University, Australia.

Lu–Hf isotope dilution analyses were conducted in the same laboratory using MC ICP-MS *Neptune*. Details on short and long term precision as well as constants used for data reduction are reported in the footnote to Table 2. The description of chemical sample treatment is presented in Anczkiewicz et al. (2004) and mass spectrometry procedures are similar to those given in Thirlwall and Anczkiewicz (2004). Age and $^{176}Hf/^{177}Hf$ initial ratio calculations were conducted by Isoplot 4.15 (Ludwig, 2008). Age errors are given at 95% confidence level.

4. Trace element analyses

Major element mapping of garnets from all the metamorphic zones studied here are presented in Dasgupta et al. (2009). They show the expected pattern, i.e. prograde growth zonation up to the kyanite grade and different extents of diffusive modification, up to complete homogenization at higher grades. Resorption is more pronounced with rising temperature and becomes substantial in

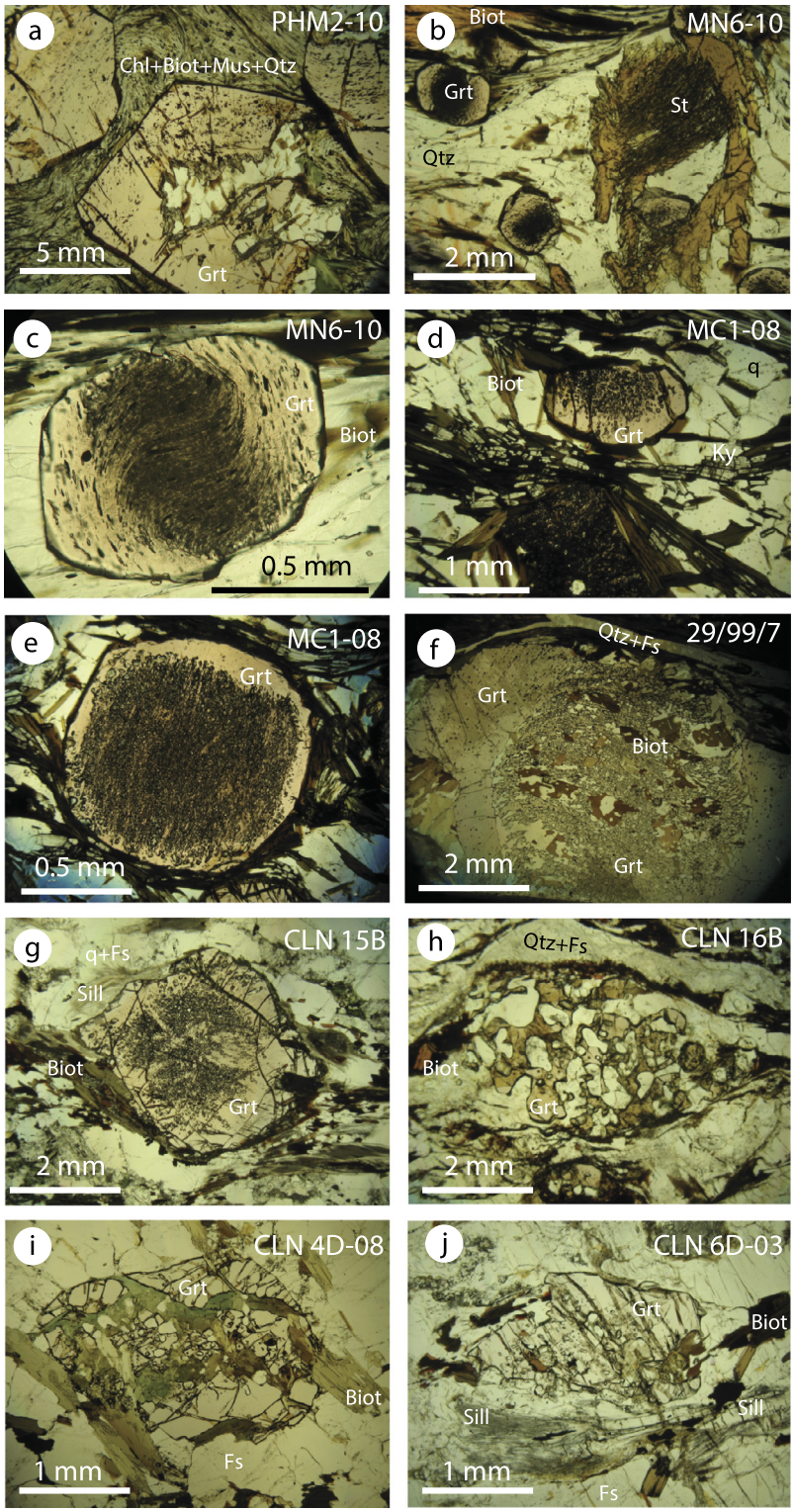

Fig. 2. Photomicrographs of garnets from the Lesser Himalaya (a–g), Main Central Thrust zone (h) and Higher Himalaya (i–j). Samples representing Barrow's zones in the Lesser Himalaya are shown in (a) garnet zone, (b and c) staurolite zone, (d and e) kyanite zone, (f) sillimanite zone and (g) muscovite-out zone. With the exception of the garnet zone where inclusions in garnet are fairly uniformly distributed (a), garnets from all other zones show broad poikilitic cores with narrow, inclusion-poor rims (b–g). In contrast, samples from the Main Central Thrust zone and Higher Himalaya are poorer in inclusions, do not show regular internal texture and are significantly resorbed (h–j). Abbreviations after Kretz (1983). See text for details.

the Higher Himalayan rocks. Details on reactions driving resorption in the studied area are given in Sorcar et al. (2014).

While major element zoning in low grade rocks is typically sufficient to support age interpretation, above the kyanite grade trace elements are usually of greater help. Since Hafnium is strongly incompatible in garnet and diffuses considerably more slowly than the heavy REE (Bloch et al., 2010), we focus our attention on Lu zonation in all metamorphic zones (Fig. 3). Nearly all garnets from the LH rocks, up to the base of the MCT zone, show a Rayleigh-like Lu zonation pattern with decreasing content from core to rim

Table 2
Summary of the Lu–Hf and Sm–Nd dating results.

Fraction	Weight (mg)	Lu (ppm)	Hf (ppm)	$^{176}Lu/^{177}Hf$	$^{176}Hf/^{177}Hf$	Age (Ma)
Garnet–mica schist, sample 24/99 GPS: N 27°27.292′E 88°31.63′						
WR	95.9	0.309	0.066	0.6599	0.282406 ± 22	10.59 ± 0.16
GRT A	47.4	9.020	0.147	8.7048	0.284007 ± 29	
GRT B	49.9	6.736	0.100	9.5640	0.284164 ± 14	
Garnet–mica schist, sample PHM2-10, GPS: N 27°27.813′E 88°31.408′						
GRT 2A	97	9.139	0.169	7.6676	0.284092 ± 30	11.05 ± 0.26
GRT 2B	95	5.808	0.151	5.4571	0.283616 ± 14	
GRT 2C	98	6.601	0.414	2.2567	0.282964 ± 13	
Garnet–staurolite schist, sample MN6-10 N 27°30.668′E 88°31.802′						
GRT B	94.4	3.403	0.116	4.1669	0.283181 ± 13	12.79 ± 0.31
GRT A	61.5	0.971	0.036	3.8417	0.283103 ± 20	
WR	97.59	0.689	0.089	1.0944	0.282447 ± 13	
Kyanite–mica schist, sample MC1-08 GPS: N 27°30.580′E 88°33.969′						
WR	103.2	0.179	0.047	0.5364	0.282354 ± 12	13.68 ± 0.19
Grt CORE	60	7.558	0.137	7.7890	0.284186 ± 32	
MID D	120	3.295	0.113	4.1165	0.283278 ± 17	
MID C	96	3.259	0.103	4.4763	0.283354 ± 24	
MID B	103	3.167	0.121	3.6940	0.283184 ± 24	
MID A	130	5.116	0.126	5.7239	0.283689 ± 27	
RIM 1	64	1.271	0.186	0.9660	0.282433 ± 29	9.9 ± 3.8
RIM 2	29.2	14.609	3.582	0.5768	0.282365 ± 13	
Garnet–silimanite gneiss, sample 29/99/7 GPS: N 27°31.757′E 88°36.369′						
GRT C	48.86	10.533	0.070	21.4435	0.287812 ± 23	14.603 ± 0.072
GRT A	51.01	12.156	0.093	18.4420	0.286975 ± 14	
WR	93.17	0.241	0.093	0.3661	0.282054 ± 14	
Garnet–sillimanite gneiss (muscovite out) CLN15B-08B GPS: N 27°36.621′E 88°38.281′						
GRT B	72.01	4.719	0.066	10.0500	0.285190 ± 10	16.759 ± 0.094
GRT A	67.95	4.225	0.067	8.9688	0.284868 ± 10	
GRT C	65.73	5.604	0.065	12.2561	0.285884 ± 13	
WR	93	0.289	0.082	0.4987	0.282207 ± 7	
Garnet–augen gneiss (Chumthang gneiss) CLN 16B-08 GPS: N 27°37.913′E 88°37.201′						
WR	107	0.347	0.039	1.2609	0.283008 ± 12	22.58 ± 0.12
GRT C	50.81	10.824	0.133	11.5418	0.287344 ± 14	
GRT A	38.96	10.498	0.133	11.1874	0.287192 ± 13	
Migmatite, sample CLN4D-08B N 27°41.366′E 88°35.148′						
WR	89.63	1.006	1.372	0.1037	0.283217 ± 12	28.071 ± 0.096
GRT B	71.83	6.542	0.069	13.3738	0.290181 ± 10	
GRT C	71.77	6.320	0.066	13.5227	0.290271 ± 12	
GRT A	63.69	6.253	0.066	13.3423	0.290129 ± 12	
Migmatite sample CLN 6D-03 GPS: N 27°42.247′E 88°33.727′						
GRT A	97.59	4.219	0.099	6.0025	0.285649 ± 19	26.44 ± 0.43
GRT B	50.02	5.799	0.076	10.7525	0.287995 ± 16	
GRT C	46.71	5.850	0.100	8.2518	0.286756 ± 16	

Notes: All errors are 2 SE (standard errors) and relate to the last significant digits. $^{176}Lu/^{177}Hf$ errors are 0.5%, JMC475 yielded 0.282159 ± 13 ($n = 21$) over the period of analyses, which is the same as our long term reproducibility calculated for 4 years period 0.282159 ± 13 ($n = 133$). Where *in run* errors were smaller than the external precision, the errors were propagated. Mass bias correction to $^{179}Hf/^{177}Hf = 0.7325$. Decay constant $\lambda_{^{176}Lu} = 1.865 \times 10^{-11}$ yr^{-1} (Scherer et al., 2001). Weights of the garnet fractions from samples MC1-08 and PHM2-10 are only approximate, taken before sulphuric acid leaching.

(Holister, 1966; Kohn, 2009; Lapen et al., 2003), which is an indication of having developed during the prograde garnet growth (Fig. 3a, b). An exception is the sillimanite grade garnet which displays high and fairly uniform Lu enrichment across a large core surrounded by a Lu-poor rim (Fig. 3b). This can be due to the contemporaneous crystallization of garnet core with another mineral with a strong preference for incorporating Lu, such as xenotime (Anczkiewicz et al., 2012; Pyle and Spear, 1999). The key observation from the perspective of our study is that all LH garnets contain strongly Lu-enriched cores that dominate Lu–Hf dating (see below). The Lu zoning patterns found in garnets from the MCT zone and from the Higher Himalayan samples bear a more complex record. The compositional variations between core and rim are smaller than in the low temperature LH garnets and the patterns are more variable even on the thin section scale (Fig. 3c, d). This is best manifested in sample CLN6D-03, where zoning profiles vary from the bell-shape (analogous to the low temperature garnets in the LH), to nearly completely flat with reacted rims (Fig. 3c). Overall, the lack of consistency of Lu zonation in the Higher Himalayan rocks does not allow an unequivocal interpretation of their origin. However, the HH garnets contain K-feldspar inclusions which must have been formed as a result of melt producing reactions. This indicates that these garnet grains recrystallized in the presence of melt, even though garnet must have formed during the early prograde evolution (see Sorcar et al., 2014 for more details). Notably, multiphase (mainly quartzofeldspathic ± biotite) inclusions are found distributed uniformly all over the garnet grains in some of the HH samples. These may be crystallized melt inclusions (e.g. Cesare et al., 2009), again suggesting that all of the garnet recrystallized in the presence of melt. Such recrystallization would explain the very diverse range of the Lu zoning patterns found in garnets from these high temperature migmatitic rocks.

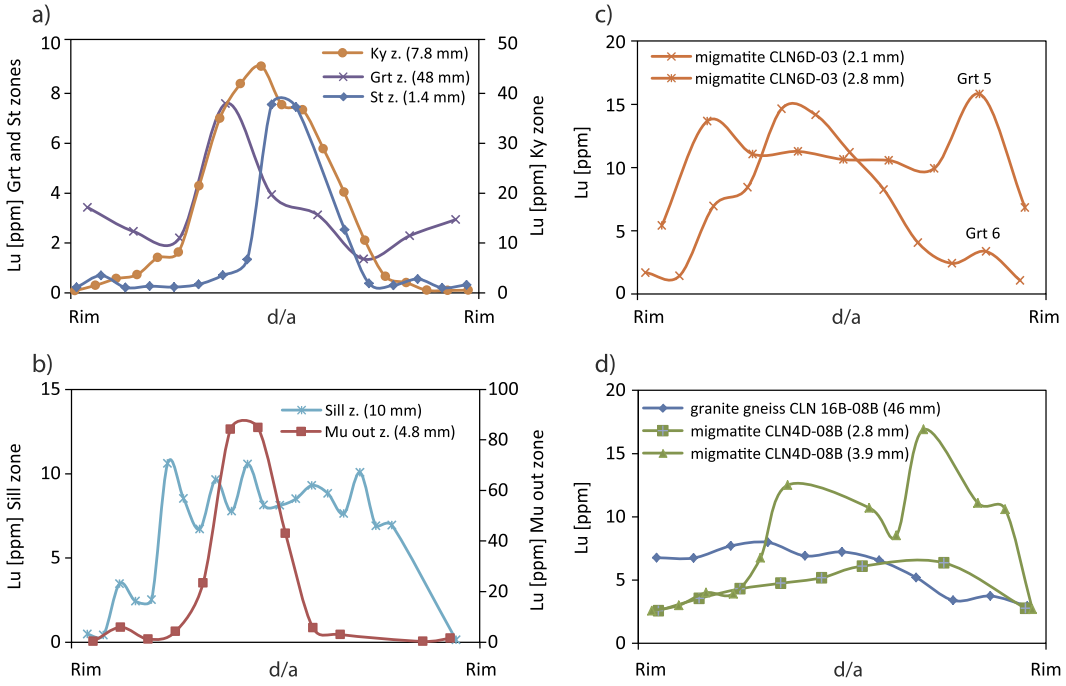

Fig. 3. Rim-to-rim normalized Lu zoning profiles in garnets from the Lesser Himalaya (a and b), from the MCT zone and the Higher Himalaya (c and d). Profile lengths are provided in the brackets next to sample label. Abbreviations: d – length of the measured Lu profile, a – diameter of the respective garnet grain, z – zone, mineral abbreviations after (Kretz, 1983).

5. Lu–Hf dating results

The Lu–Hf dating results are summarized in Table 2 and in Figs. 4–6. We describe below the isotope systematics and the obtained ages progressing from the southern, structurally deeper part of the sequence to the northern, structurally higher levels and higher metamorphic grades. All analyzed garnet fractions are characterized by high $^{176}Lu/^{177}Hf$ and $^{176}Hf/^{177}Hf$ ratios, which along with the little scatter of data (MSWD $\leq$ 1.7) observed for individual isochrons, allowed high precision ages to be obtained. In isochron diagrams (Figs. 4 and 6) we quote ages as calculated by Isoplot (Ludwig, 2008), which well illustrates the analytical potential of the technique, but throughout the text the dates were rounded to fewer decimal places, which seems more reasonable after taking the geological context into account (see below). The Hafnium concentrations determined by isotope dilution (ID) in all garnets are at sub ppm level, which is typical of most metamorphic rocks and indicates that the analyzed fractions were not significantly influenced by Hf-rich inclusions (Table 2).

Two samples were dated from the garnet zone. Sample 24/99 was dated using bulk garnet separates and yielded 10.6 $\pm$ 0.2 Ma age (Fig. 4a). Three fractions prepared from a single garnet crystal from sample PHM2-10 (see above) define an isochron age of 11.1 $\pm$ 0.3 Ma (Fig. 4b). The large spread of the $^{176}Lu/^{177}Hf$ ratios among different fractions is a result of random mixing of Lu-rich core with Lu-poor rim end members rather than due to the presence of inclusions (mainly mica and quartz) that do not substantially contribute to the Lu and Hf budget. This explanation can be extended to samples from other metamorphic grades that show large variations in $^{176}Lu/^{177}Hf$ ratios among garnet fractions, but still define highly precise ages (see below).

Sample MN6-10, from the staurolite zone, was dated at 12.8 $\pm$ 0.3 Ma (Fig. 4c). A kyanite zone sample was used for high spatial resolution single crystal dating due to the presence of sufficiently large garnets. Three different zones within the garnet were split into 7 fractions (Fig. 5a). Two growth zones were selected within the garnet core which is marked by the presence of sigmoidal inclusion trails (fractions: “center” and “mid A–D”). The third zone is defined by the inclusions poor garnet rim (fractions “rim A–B”). The fraction labeled “center” represents the geometric center of the crystal and coincides with the highest Mn and Lu content that mark the zone of the initial prograde growth (Fig. 5b, c). Four fractions labeled “mid A–D” were prepared out of the intermediate area between the geometric center and the garnet rim (Fig. 5a). Fragments of rim that were too thin for cutting out were abraded away in order to eliminate contamination of the neighboring “mid” zone (Fig. 5a). Whole rock composition was used for initial $^{176}Hf/^{177}Hf$ ratio correction for all garnet fractions.

As expected, the highest isotopic ratios were obtained for the “center” fraction which shows the highest enrichment in Lu (Fig. 5b). All “mid” fractions gave lower isotopic ratios but were indistinguishable from the “center” fraction in terms of age. Ages calculated for individual garnet-whole rock tie lines show a span of <0.6 Ma (Fig. 4d). They do not show any correlation with the $^{176}Lu/^{177}Hf$ ratios which would be expected in the case of slowly crystallizing garnet with decreasing Lu content towards the rim. Instead, ages of individual garnet fractions represent random scatter that reflects analytical uncertainty. All fractions together with the whole rock define a precise isochron age of 13.7 $\pm$ 0.2 Ma (Fig. 4d).

The two rim fractions representing a later growth phase yielded low isotopic ratios precluding high age precision to be obtained. Such low ratios, however, are expected for the Lu-poor rim (Fig. 4e, f and Fig. 5a, b). Despite the fact that a precise age could not be determined, both rim fractions together with the whole rock data define a distinctly younger age of 9.9 $\pm$ 3.8 Ma.

The age of the sillimanite zone garnet (sample 29-99-7) is defined by the two fractions with the highest $^{176}Lu/^{177}Hf$ ratios and the whole rock. These yield an isochron age of 14.6 $\pm$ 0.1 Ma (Fig. 4g).

Further up the section, in the vicinity of Chungthang town, sample CLN 15B-08 marking the beginning of muscovite dehydra-

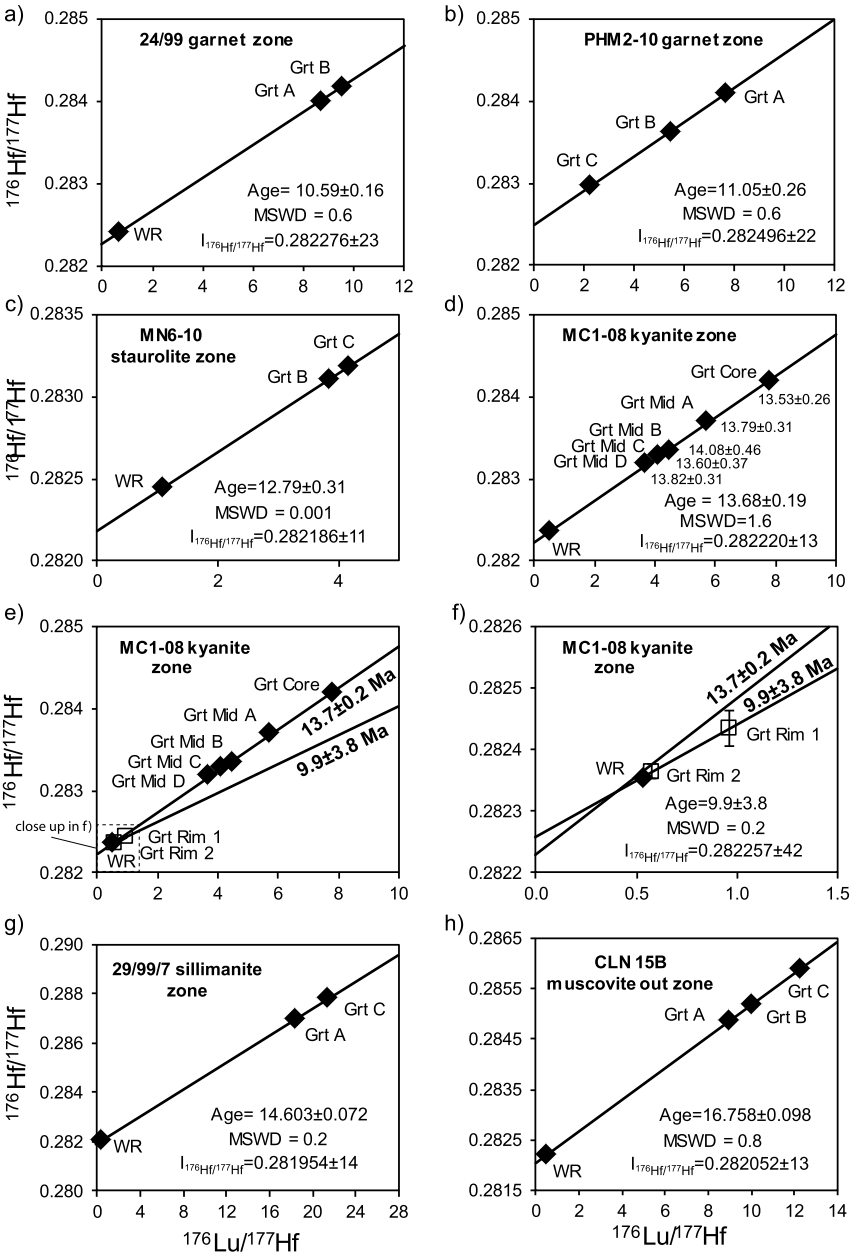

Fig. 4. Lu–Hf isochron diagrams of samples from the Barrovian metamorphic zones in the Lesser Himalaya. Samples 24-99 and PHM2-10 are from the garnet zone (a and b, respectively), while sample MN6-10 represents staurolite zone (c). Sample MC1-08 comes from the kyanite zone and was subjected to high spatial resolution dating (d). Garnet fraction labels correspond to those shown in Fig. 3a. Ages calculated for the individual whole rock–garnet–core fractions are given next to the corresponding marks and labels (d). Two rim analyses of the same garnet are shown in (e). Small dashed rectangle at the bottom left marks close up shown in (f). Sillimanite and muscovite-out zones are represented by samples CLN15B and 29/99/7 (g and h, respectively). Abbreviations: WR – whole rock, Grt – garnet, Mid A–D – garnet fractions (see also Fig. 3a). Errors are smaller than the size of the marks. See text for details.

tion melting (Dasgupta et al., 2009) gave an age of 16.8 ± 0.1 Ma (Fig. 4h). This location is at the very top of the Lesser Himalayan sequence in the studied section.

Dating of garnets from the highly sheared garnet granite–gneiss (known as Chungthang granite–gneiss), positioned about 3 km further to the NW along the Teesta river within the MCT zone (CLN 16B-08), yielded an age of 22.6 ± 0.1 Ma (Fig. 6a). Two migmatite samples (CLN4D-08 and CLN6D-03) located well within the lower part of the Higher Himalayan section (Fig. 1c) gave 28.1 ± 0.1 and 26.4 ± 0.4 Ma (Fig. 6b, c). It is noteworthy that the samples CLN16B-08 and CLN4D-08 both show almost the same isotopic ratios in garnets. This indicates little variation in Lu zonation in garnet at least on hand specimen scale (Fig. 6a, b).

6. Interpretation

6.1. High age precision

The high analytical precision of the ages obtained in this study is best demonstrated by the Isoplot calculations (Ludwig, 2008) that estimate uncertainties at 95% confidence level to the second and even third decimal place (thousands of years). The estimates take into account external reproducibility established with the repeated measurements of the JMC 475 standard, although this is typically better than the in-run errors obtained for rather small amount (typically about 5 ng) of Hf present in garnet analyses (Table 2). Such high precision reflects present day analytical po-

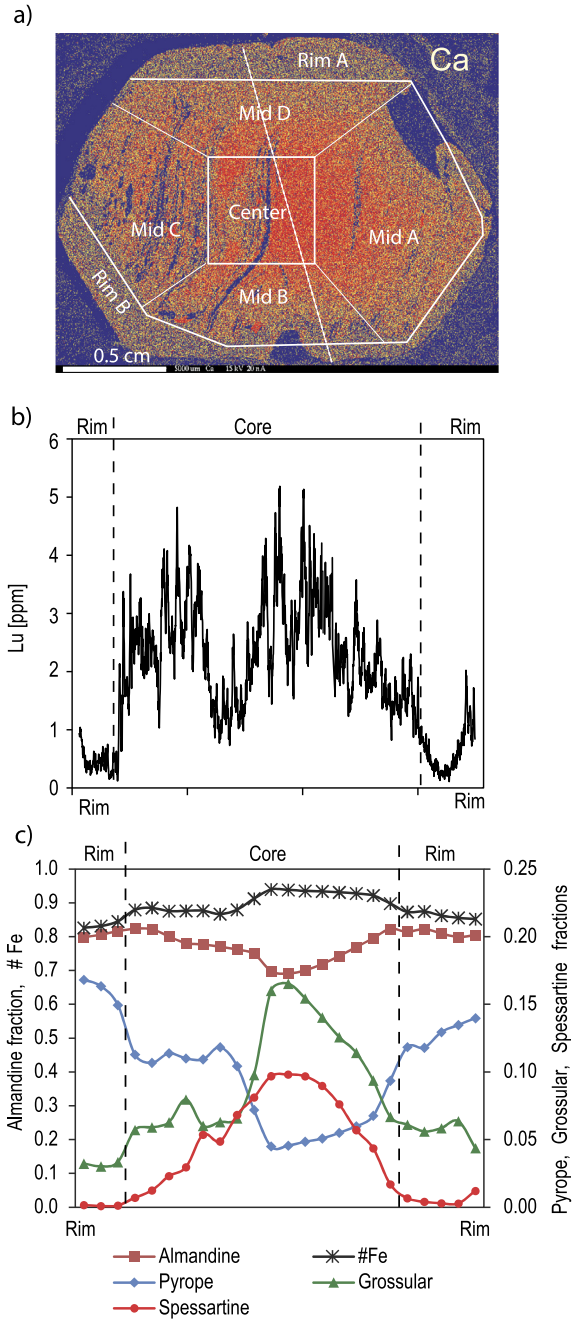

Fig. 5. Internal texture and Ca-compositional X-ray map of MC1-08 garnet subjected to high resolution dating. Broad poikilitic core shows sigmoidal inclusion trails surrounded by inclusion-poor rim, which correlate with Ca zonation (a). Within the core two growth zones were selected: "center" corresponding to geometric center of the crystal and "mid" – representing intermediate zone between "center" and "rim" (a). Rim areas too thin to be cut out for isotope dilution (ID) analyses were abraded away. Solid lines mark cutting trails along which the crystal was divided into individual fractions that were subjected to Lu–Hf dating (a). Labels correspond to those in Fig. 4d–f and Table 2. Dashed line in (a) marks LA ICP-MS scan along which Lu abundance presented in (b) was determined. Lu shows enrichment in the core and depletion in the rim that is typical of prograde growth of garnet, which correlates with major element distribution presented in c). Small Lu depletion observed near the core is due to higher inclusion content which affected the analyses.

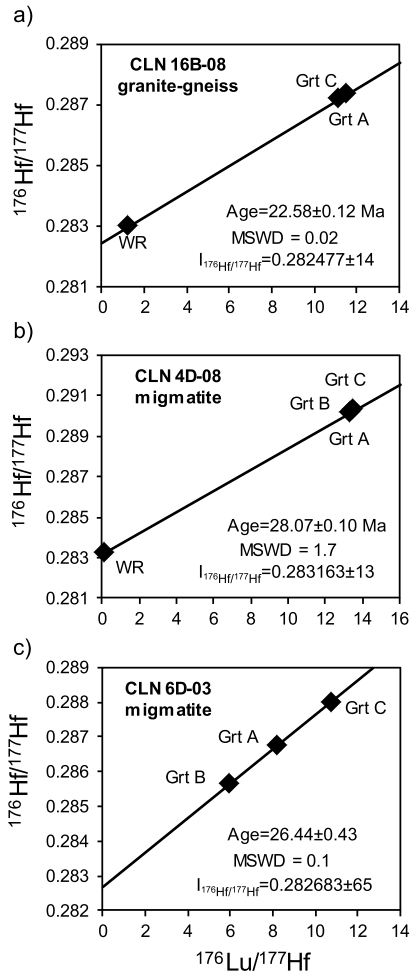

Fig. 6. Lu–Hf isochron diagrams for the granite-gneiss from the MCT zone (a) and for the Higher Himalayan migmatites (b and c). Abbreviations: WR – whole rock, Grt – garnet. Errors are smaller than the size of point marks. See text for details.

tential rather than real uncertainty of garnet dates. Critical factors that control the "true" precision of garnet ages are the geological aspects that typically cannot be quantified. The most obvious example of such a factor is the duration of garnet growth. This can be long lasting and would typically be undetected by the average age produced by the bulk garnet dating technique. The only method that allows this problem to be overcome is high spatial resolution dating. Previous high resolution garnet dating demonstrated that a single crystal growth may last up to several million years (e.g. Christensen et al., 1989; Pollington and Baxter, 2011; Vance and Onions, 1992). Those estimates are based on the Rb–Sr and Sm–Nd dating of crystal fragments of different growth zones, which is possible only if a crystal is large enough. Our high resolution Lu–Hf dating conducted on a garnet from the kyanite grade mica schist shows that the growth of the inclusion-rich internal part of garnet (about 90% of total garnet) was fast. Rapid crystallization is indicated by the unresolvable age differences between the "center" and the "mid" fractions that represent different growth (time) zones. Additional argument supporting fast garnet crystallization in the studied samples is high precision of ages obtained for the samples where garnets yield a large spread in $^{176}Lu/^{177}Hf$ ratios (Fig. 4). As mentioned above, the spread is caused by various proportions of core and rim in the bulk garnet separates. In the case of slow garnet crystallization large age differences between garnet center and the more external zones would cause excess scatter in the measured isotopic ratios among the garnet fractions, which in turn would prevent obtaining a high precision age.

Thus, we conclude that early garnet growth that can be correlated with the inclusion rich cores was fast, and a geologically meaningful resolution of $\leq$0.5 Ma would be a conservative estimate in the studied samples.

The results of our high resolution core-rim dating indicate another important issue that is central to the use of bulk garnet dating: Lu-depleted rims that are even a few million years younger do not greatly influence bulk separate dating. This is a consequence of a simple mass balance. Considerably higher $^{176}Lu/^{177}Hf$ ratios in cores are not significantly influenced by little radiogenic rims (see also modeling results of Lapen et al., 2003).

6.2. Lesser Himalaya

Garnets up to the sillimanite zone share several features in common. They are all rather well preserved and their centers are rich in inclusions that show preferred orientation expressed as sigmoidal or straight inclusion trails (their origin is beyond the scope of the present study and will not be considered further). This fabric is less intense in the garnet zone but is still clearly detectable (Fig. 2a–f). In the sillimanite grade sample collected from the top of the LH sequence (CLN15B-08), the garnet core also contains abundant inclusions. However, unlike in samples from the structurally lower levels, they do not show any preferred orientation (Fig. 2g).

The Lu content determined by isotope dilution (Table 2) is found to be approximately an average of the Lu concentrations obtained along the profiles determined by LA ICP-MS (Fig. 3). This shows that despite the occurrence of poikiloblastic cores, sample preparation did not bias garnet separates towards cleaner rims. Such bias would result in a huge loss of precision due to reduction in $^{176}Lu/^{177}Hf$ ratios (a good example of which is the rim of sample MC1-08). The important consequence is that nearly all our garnet ages do not date the metamorphic peak, which is represented by the rims in these relatively low grade ($<$c. 600 °C) rocks. As mentioned above, all samples below the MCT (including CLN 15B-08) have garnet cores strongly enriched in Lu relatively to their rims, and thus the core regions dominated the Lu–Hf dating (Fig. 3a–b). Preservation of the prograde Lu fractionation patterns implies that the Lu–Hf dates correspond to the age of formation of garnet cores, i.e. the crossing of the garnet isograd condition by a given rock during its prograde history.

The only exception to the interpretation presented above is the 9.9 ± 3.8 Ma age obtained for garnet rim from the kyanite zone. This age is interpreted as the time of peak kyanite grade metamorphism, as indicated by the major element zoning pattern shown in Fig. 5c. This younger age (relatively to 13.7 ± 0.2 Ma of garnet core) may reflect either a later growth phase along the same metamorphic P–T path, or a slow-down in the pace of garnet crystallization. Our data do not allow discriminating between these two options.

It is noteworthy that the youngest ages obtained for the garnet zone, although in a strict sense represent the time of prograde growth, closely approximate metamorphic peak conditions. This is due to the fact that the metamorphic peak conditions did not significantly exceed the conditions of the first garnet growth in these rocks and garnet crystallization occurred over a very narrow P–T range within a short time span (see above).

6.3. Higher Himalaya

Unlike garnets from the Lesser Himalaya, garnets in the HH samples are sub- or anhedral and often show strong resorption (Fig. 2h–j) due to breakdown reactions occurring during prolonged melting, decompression and back-reaction of melts (Rubatto et al., 2013; Sorcar et al., 2014). These garnets differ in their trace element zoning patterns as well (Fig. 3c, d). The growth zoning patterns showing strong fractionation of HREE at the core are largely lost through a combination of diffusion, and more importantly recrystallization, at high temperatures (see above). Lu growth zonation can be rarely found in some larger garnets from CLN6D-03 (Fig. 3c). However, in general, the trace element zonation patterns in garnets from the studied samples alone do not add a strong constraint on age interpretation. As discussed above, the presence of K-feldspar and multiphase quartzofeldspathic inclusions (interpreted to be melts) even in the cores of some garnets from the HH region indicate that the garnet crystals in these rocks formed near peak conditions in the presence of melt. Thus, the Lu–Hf dates obtained for the HH rocks are interpreted as reflecting peak metamorphic conditions. This inference is supported by comparison with monazite dates of Rubatto et al. (2013). The latter authors concluded that the main melting episode related to biotite dehydration and abundant feldspar crystallization occurred between 28 and 25 Ma in the area south of Lachen (Fig. 1b, c). They used the presence of K-feldspar inclusions in monazite and strong Eu anomaly as evidence of monazite crystallization in the presence of melt near the metamorphic peak. As a matter of fact, sample CLN6D-03 is the same sample that was used for U–Pb monazite dating by Rubatto et al. (2013). Our 26.4 ± 0.4 Ma Lu–Hf age is in excellent agreement with the 28–25 Ma time span proposed for this melting episode on the basis of monazite dates.

Unlike all other metasedimentary samples, CLN16B-08 represents the Chungthang granite gneiss that stems from an older granitic protolith and is located within the MCT zone. So far, petrological studies of these rocks have been very limited, and thus the significance of its age (22.6 ± 0.1 Ma) is more difficult to place. Nevertheless, the Lu zoning patterns in garnets from this sample are similar to those from the other higher temperature HH rocks. Therefore, the date also likely refers to the metamorphic peak.

7. Discussion

The Lu–Hf garnet dates presented in this study are consistent with previously published ages from the Sikkim Himalaya. As noted already, LH ages of 11–17 Ma, and of 23 Ma in the MCT zone are largely consistent with the Th–Pb monazite ages of Catlos et al. (2004). Dates between 26 and 28 Ma from the High Himalayan rocks also lie within the wide spread of ages obtained by Catlos et al. (2004) and Rubatto et al. (2013) who conducted U–Pb monazite and zircon dating. The latter authors found strong local variations in the timing of anatexis in the HH that spread over the period of 31–15 Ma. Our garnet dates are consistent with that observation. In particular, as noted above, the inferred age of peak metamorphism of 26–28 Ma for the sample CLN6D-03 is in excellent agreement with 26.4 ± 0.4 Ma and 28.1 ± 0.1 Ma garnet ages obtained in this study. Harris et al. (2004) dated a garnet from a HH migmatite in West Sikkim and determined Sm–Nd ages of 23 ± 3 Ma for the garnet core (their inferred peak pressure of metamorphism) and 16 ± 2 Ma for the rim (their inferred decompression and melting). The latter age is significantly younger than garnet ages obtained in this study but is close to the end of the melting period within the HH postulated by Rubatto et al. (2013). Similarly, early garnet growth dated at 23 ± 3 Ma is slightly later than in the northern section investigated in this study. This suggests that in West Sikkim the timing of metamorphism could have been somewhat different.

The Lu–Hf ages that we have obtained for the LH metasediments constrain the duration of prograde metamorphism (using first garnet growth as a marker) across the sequence. They display a remarkably consistent pattern of decreasing ages from the structurally higher (sillimanite grade) to the structurally lower (garnet grade) rocks (Fig. 1c). The time limits are set by the youngest, garnet grade rocks at the bottom of the sequence which are dated at 10.6 ± 0.2 Ma and by the sillimanite grade rocks (within muscovite breakdown zone) at the top of the LH succession dated at 16.8 ± 0.1 Ma. This gives a $\sim$6 million year time interval over

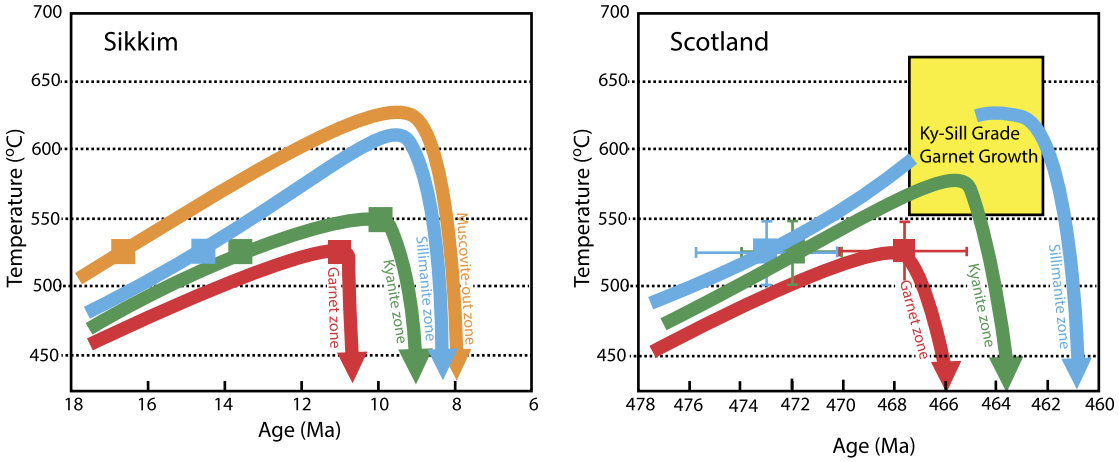

Fig. 7. Comparison of temperature–time paths for the Barrow's zones in the inverted sequence in Sikkim (this study) and non-inverted sequence in Scotland (Baxter et al., 2002). Temperature estimates for the Sikkim rocks based on the study of Dasgupta et al. (2009). Both regions show progressively younger prograde garnet formation ages with decreasing metamorphic grade and display a fairly narrow time range during which peak metamorphism was achieved.

which the garnet isograd was passed by the entire Barrovian sequence. Since there is little structural data for the upper part of the sillimanite zone (directly below the MCT), some caution is needed while treating the sequence as strictly coherent from garnet-in until the muscovite-out zone. Nevertheless, the general similarity of the sample CLN16B-08 in terms of texture and protolith age to the other LH rocks and the lack of significant time gap indicate that it still belongs to the upper part of the LH sequence. Some disruption of the LH continuity is caused by the Mangan Thrust (MCT1 of Catlos et al., 2004). However, this fault is entirely within the staurolite zone and neither cuts out nor repeats any significant part of the sequence. These rather small disruptions do not significantly affect the studied LH sequence in Sikkim which is uniquely coherent on a whole orogen scale. This makes the Sikkim region very suitable for determining rates and duration of metamorphism in the Himalaya.

Our dating results demonstrate that the ages of prograde metamorphism show a normal correlation with PT conditions (in higher grade rocks garnet growth was initiated earlier and thus growth ages are older) but in their present position they support an overall inversion in the "structural sense". A similar age inversion has already been inferred from monazite dating in the Nepal Himalaya (Catlos et al., 2001), although in Sikkim the Th–Pb monazite dates do not show as systematic changes as a function of metamorphic grade (Catlos et al., 2004).

In a classic Barrovian sequence in Scotland, prograde metamorphic Sm–Nd garnet ages show younger garnet growth in progressively lower metamorphic grades (Baxter et al., 2002), as in this study (Fig. 7). Additionally, the latter authors document about 5 Ma time difference in crossing the garnet isograd, between garnet and sillimanite zones. Taking into account that time resolution achievable by the Sm–Nd system is much smaller than the Lu–Hf method obtained in this study, the estimates of the latter authors compare well with 4 Ma time difference reported here for analogous grades in Sikkim (to make the comparison more exact, we omitted sample CLN 15B-08 representing muscovite-out zone, which was not studied in the Scottish sequence). The timing of peak metamorphic conditions established by Baxter et al. (2002) for the same samples were not resolvable by the Sm–Nd method and hence the data were interpreted as indicating practically contemporaneous peak temperature in garnet, staurolite and sillimanite zones that occurred within 2.8 ± 3.7 Ma. In general, the Lu–Hf method cannot date the metamorphic peak in the studied LH rocks. However, in the case of garnet zone, the time of prograde garnet growth and the metamorphic peak are nearly contemporaneous in such a quickly evolving setting. A special case is kyanite zone garnet rim dating, which indeed corresponds to the metamorphic peak. Our geochronological data obtained for rocks from these two metamorphic grades indicate that the peak metamorphism in the garnet zone (dated at ~11 Ma) and in the kyanite zone (dated at 9.9 ± 3.8 Ma) occurred within a very narrow time span. Unfortunately, we were unable to determine the time of the peak sillimanite grade metamorphism. Nevertheless, the overall age pattern in Sikkim and Scotland is almost the same, i.e. (a) older garnet formation ages are found in higher metamorphic grade rocks and (b) peak metamorphism occurred within a short time span in all Barrow's zones (Fig. 7). Thus, the difference between the two regions is limited to the "metamorphic polarity" of the Sikkim sequence (higher PT at shallower structural levels). This leads us to suggest that metamorphic inversion in the Sikkim area occurred after thermal climax, as also predicted by the thermomechanical model of Faccenda et al. (2008) described below.

8. Tectonic implications for the Sikkim Himalaya

A thermomechanical geodynamic model of continental collision proposed by Faccenda et al. (2008) captures many of the features observed for the LH rocks of Sikkim. The model calculates thermal and mechanical evolution of a region, where two lithospheric plates converge, according to flow laws by solving the equations of conservation of energy, momentum and mass. The most relevant consequence of their model, that is testable with the present work, is the prediction of relative timing and duration of regional metamorphism. If the average temperature at which garnet grows in pelitic rocks is taken to be ~500 °C, then the time at which this isotherm is crossed by various markers in the model that constitute a coherent, inverted sequence can be compared to the dates determined in this study. Fig. 8 shows the P–T–t evolution of markers that constitute a Barrovian sequence (Faccenda et al., 2008). The thin lines describe the P–T–t paths followed by each marker (e.g individual rock) and the heavy lines are iso-time curves, i.e. a curve that connects all markers at a given point of time. Therefore, the continuity of the heavy lines represents the geometry of the coherent block during burial and exhumation. It is found that in this model the heavy lines (a) remain coherent and (b) are buried and exhumed such that the rocks metamorphosed at higher grades are found closer to the point of collision after exhumation (accounting for a dip toward the collision point – north in the case of the Himalaya – this implies higher grade rocks would occur toward the structural top). Notably, in the

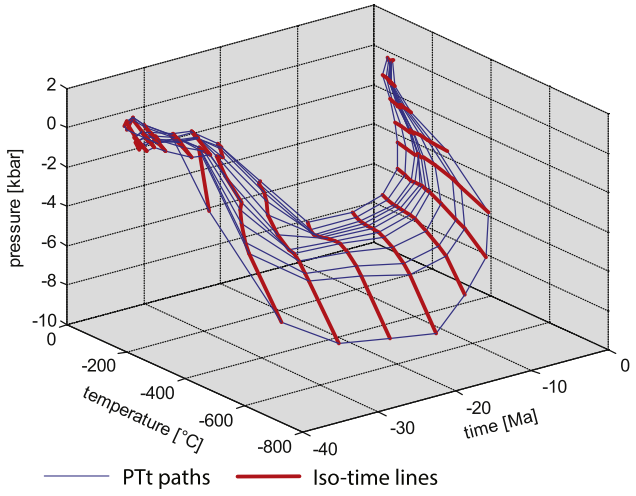

Fig. 8. P–T–t paths based on the thermomechanical models of Faccenda et al. (2008). Modeling conditions: convergence velocity: 7 cm/year, a lower crustal rheology corresponding to that of an anorthitic plagioclase, heat generation: 4 $\mu W/m^3$. This set of conditions is very close to the ones used for the basis model, and illustrated in Figs. 2–5 of Faccenda et al. (2008). See text for details.

context of this study, it is found that: 1) higher grade rocks cross a given isotherm along the prograde path earlier than lower grade rocks, 2) the time difference between rocks that ultimately attain c. 600 °C and those that attain c. 500 °C is about 4 Ma, and 3) the time at which peak metamorphism is attained, is very similar for rocks of all grades. This is consistent with our estimates and with the observation of Baxter et al. (2002) made for Barrow's zones in Glen Clova region of Scotland. In this simple, one stage geodynamic model the rocks reach the surface after about 30 Ma of initiation of collision. This is a little too soon for the LH rocks (metamorphism at 10–17 Ma, after initiation of collision at ~55 Ma), but the development of more sophisticated models may remove this discrepancy. The ability to produce a coherent sequence inverted in terms of pressure and temperature of metamorphism as well as timing of garnet growth indicates that the models of Faccenda et al. (2008) provide a good first order description of the geodynamic scenario that produced the LH rocks in Sikkim. Important details such as the age of HH vs. LH metamorphism in the rocks exposed at the surface today and the timing of exhumation remain to be adequately modeled.

9. Conclusions

The Sikkim Himalaya in NE India expose a uniquely well preserved and petrologically continuous metasedimentary sequence that enabled us to investigate Lu–Hf isotope systematics in gradually higher metamorphic grade rocks from the first appearance of garnet at c. 500 °C in the Lesser Himalaya to biotite dehydration melting at c. 800 °C in the Higher Himalaya.

The prograde garnet formation ages obtained for the LH become progressively older with decreasing structural depth and range from 10.6 ± 0.2 Ma in garnet zone to 16.8 ± 0.1 Ma in muscovite dehydration zone. These ages constrain the timing and duration of the Barrovian sequence formation, which lasted about ~6 Ma. The age pattern is inverted but shows "normal" correlation with metamorphic grade, i.e. earlier garnet growth in higher grade rocks. Indistinguishable within error ages of peak metamorphic conditions obtained for the garnet and kyanite zones suggest that thermal climax likely occurred in the whole sequence within a relatively short time span between ~10 and 13 Ma. Such an age pattern is analogous to that observed in the non-inverted Barrovian sequence in Scotland (Baxter et al., 2002), which suggests that the Sikkim sequence was produced in a similar manner and that inversion of metamorphic polarity occurred after the metamorphic peak was attained in all grades.

Dating of high grade migmatites from the overthrust Higher Himalaya resulted in even older dates, however, they do not show age progression continuous with that observed in the LH. Instead, there is a 6 Ma jump to 22.6 ± 0.1 Ma age for the sample from within the MCT zone and even older ages of 28.1 ± 0.1 and 26.4 ± 0.4 Ma were obtained for the structurally lower part of the HH. Unlike in LH garnets, the Lu–Hf system in HH garnets records melting at or near thermal peak conditions.

The age pattern obtained in this study is in accord with the thermomechanical model of continental collision by Faccenda et al. (2008). Their results predict early and diachronous anatexis within the more "disordered" Higher Himalaya whereas the Lesser Himalaya throughout their evolution behaved as a coherent unit. The model recovers our main findings for the LH showing earlier garnet growth in higher grade rocks, nearly contemporaneous attainment of peak metamorphic conditions in all grades, and post-peak inversion of the coherent block during exhumation. Our data quantifies the timing and duration of these processes which are of fundamental significance for understanding continental collision processes.

Acknowledgements

We are thankful to D. Rubatto and N. Sorcar for discussions in the field. I. Kocjan and A. Zagórska were of tremendous help with garnet separation. R. Anczkiewicz acknowledges financial support by NCN research Grant No. N N307 082137. The research of S. Chakraborty was supported by funds from DFG and the Ruhr Universität Bochum. We thank two anonymous reviewers for their comments that helped improving the manuscript.

References

Acharryya, S., Ray, K., 1977. Geology of the Darjeeling–Sikkim Himalaya, guide to excursion no. 4. In: International Gondwana Symposium. In: Geological Survey of India, vol. 25.

Anczkiewicz, R., Platt, J.P., Thirlwall, M.F., Wakabayashi, J., 2004. Franciscan subduction off to a slow start: evidence from high-precision Lu–Hf garnet ages on high grade-blocks. Earth Planet. Sci. Lett. 225, 147–161.

Anczkiewicz, R., Thirlwall, M., Alard, O., Rogers, N.W., Clark, C., 2012. Diffusional homogenization of light REE in garnet from the Day Nui Con Voi Massif in N-Vietnam: implications for Sm–Nd geochronology and timing of metamorphism in the Red River shear zone. Chem. Geol. 318, 16–30.

Barrow, G., 1893. On an intrusion of muscovite–biotite gneiss in the south-eastern highlands of Scotland, and its accompanying metamorphism. Q. J. Geol. Soc. Lond. 49, 330–354.

Baxter, E.F., Ague, J.J., Depaolo, D.J., 2002. Prograde temperature–time evolution in the Barrovian type-locality constrained by Sm/Nd garnet ages from Glen Clova, Scotland. J. Geol. Soc. 159, 71–82.

Bloch, E., Ganguly, J., Hervig, R., 2010. Diffusion kinetics of Hafnium in garnet: experimental determination and geochronological implications. In: Goldschmidt Conference Abstracts, p. A97.

Catlos, E.J., Harrison, T.M., Kohn, M.J., Grove, M., Ryerson, F.J., Manning, C.E., Upreti, B.N., 2001. Geochronologic and thermobarometric constraints on the evolution of the Main Central Thrust, central Nepal Himalaya. J. Geophys. Res., Solid Earth 106, 16177–16204.

Catlos, E.J., Dubey, C.S., Harrison, T.M., Edwards, M.A., 2004. Late Miocene movement within the Himalayan Main Central Thrust shear zone, Sikkim, north–east India. J. Metamorph. Geol. 22, 207–226.

Cesare, B.S.F., Salvioli-Mariani, E., Pedron, D., Cavallo, A., 2009. "Nanogranite" and glassy inclusions: the anatectic melt in migmatites and granulites. Geology 37, 627–630.

Christensen, J.N., Rosenfeld, J.L., Depaolo, D.J., 1989. Rates of tectonometamorphic processes from rubidium and strontium isotopes in garnet. Science 244, 1465–1469.

Dasgupta, S., Ganguly, J., Neogi, S., 2004. Inverted metamorphic sequence in the Sikkim Himalayas: crystallization history, P–T gradient and implications. J. Metamorph. Geol. 22, 395–412.

Dasgupta, S., Chakraborty, S., Neogi, S., 2009. Petrology of an inverted Barrovian sequence of metapelites in Sikkim Himalaya, India: constraints on the tectonics of inversion. J. Sci. 309, 43–84.

Faccenda, M., Gerya, T.V., Chakraborty, S., 2008. Styles of post-subduction collisional orogeny: influence of convergence velocity, crustal rheology and radiogenic heat production. Lithos 103, 257–287.

Ganguly, J., Dasgupta, S., Cheng, W.J., Neogi, S., 2000. Exhumation history of a section of the Sikkim Himalayas, India: records in the metamorphic mineral equilibria and compositional zoning of garnet. Earth Planet. Sci. Lett. 183, 471–486.

Ghosh, A., 1956. Recent advances in the geology and structure of the eastern Himalaya. In: Indian Science Congress, pp. 85–99.

Harris, N.B.W., Caddick, M., Kosler, J., Goswami, S., Vance, D., Tindle, A.G., 2004. The pressure–temperature–time path of migmatites from the Sikkim Himalaya. J. Metamorph. Geol. 22, 249–264.

Holister, L.S., 1966. Garnet zoning: an interpretation based on Rayleigh fractionation model. Science 154, 1647–1651.

Jochum, K.P., Weis, U., Stoll, B., Kuzmin, D., Yang, Q., Raczek, I., Jacob, D.E., Stracke, A., Birbaum, K., Frick, D.A., Günther, D., Enzweiler, J., 2011. Determination of reference values for NIST SRM 610-617 glasses following ISO guidelines. Geostand. Geoanal. Res. 35, 397–429.

Kellett, D.A., Grujic, D., Coutand, I., Cottle, J., Mukul, M., 2013. The South Tibetan detachment system facilitates ultra rapid cooling of granulite-facies rocks in Sikkim Himalaya. Tectonics 32, 252–270.

Kohn, M.J., 2009. Models of garnet differential geochronology. Geochim. Cosmochim. Acta 73, 170–182.

Kretz, R., 1983. Symbols for rock-forming minerals. Am. Mineral. 68, 277–279.

Lal, R., Mukherji, S., Ackermand, D., 1981. Deformation and Barrovian metamorphism at Takdah, Darjeeling (eastern Sikkim). In: Saklani, P.S. (Ed.), Metamorphic Tectonics of the Himalaya. Today and Tomorrow Publishers, Delhi, pp. 231–278.

Lapen, T.J., Johnson, C.M., Baumgartner, L.P., Mahlen, N.J., Beard, B.L., Amato, J.M., 2003. Burial rates during prograde metamorphism of an ultra-high-pressure terrane: an example from Lago di Cignana, western Alps, Italy. Earth Planet. Sci. Lett. 215, 57–72.

Ludwig, K.R., 2008. Isoplot. A Geochronological Toolkit for Microsoft Excel. Berkley Geochronology Centre, Special Publication, vol. 4, p. 77.

Mottram, C.M., Argles, T.W., Harris, N.B.W., Parrish, R.R., Horstwood, M.S.A., Warren, C.J., Gupta, S., 2014. Tectonic interleaving along the Main Central Thrust, Sikkim Himalaya. J. Geol. Soc. 171, 255–268.

Müller, W., Shelley, M., Miller, P., Broude, S., 2009. Initial performance metrics of a new custom-designed ArF excimer LA-ICPMS system coupled to a two-volume laser-ablation cell. J. Anal. At. Spectrom. 24, 209.

Mukhopadhyay et al., in preparation.

Pollington, A.D., Baxter, E.F., 2011. High precision microsampling and preparation of zoned garnet porphyroblasts for Sm–Nd geochronology. Chem. Geol. 281, 270–282.

Pyle, J.M., Spear, F.S., 1999. Yttrium zoning in garnet: coupling of major and accessory phase during metamorphic reactions. Geol. Mater. Res. 1, 1–49.

Ray, S.K., 2000. Culmination zones in eastern Himalaya.

Rubatto, D., Chakraborty, S., Dasgupta, S., 2013. Timescales of crustal melting in the Higher Himalayan Crystallines (Sikkim, Eastern Himalaya) inferred from trace element-constrained monazite and zircon chronology. Contrib. Mineral. Petrol. 165, 349–372.

Scherer, E., Munker, C., Mezger, K., 2001. Calibration of the lutetium–hafnium clock. Science 293, 683–687.

Searle, M.P., Szulc, A.G., 2005. Channel flow and ductile extrusion of the high Himalayan slab–the Kangchenjunga–Darjeeling profile, Sikkim Himalaya. J. Asian Earth Sci. 25, 173–185.

Sorcar, N., Hoppe, U., Dasgupta, S., Chakraborty, S., 2014. High-temperature cooling histories of migmatites from the High Himalayan Crystallines in Sikkim, India: rapid cooling unrelated to exhumation? Contrib. Mineral. Petrol. 167, 1–34.

Thirlwall, M.F., Anczkiewicz, R., 2004. Multidynamic isotope ratio analysis using MC–ICP–MS and the causes of secular drift in Hf, Nd and Pb isotope ratios. Int. J. Mass Spectrom. 235, 59–81.

Vance, D., Onions, R.K., 1992. Prograde and retrograde thermal histories from the central Swiss Alps. Earth Planet. Sci. Lett. 114, 113–129.

Yin, A., 2006. Cenozoic tectonic evolution of the Himalayan orogen as constrained by along-strike variation of structural geometry, exhumation history, and foreland sedimentation. Earth-Sci. Rev. 76, 1–131.